

Walk-away VSP using drill noise as a source

Jaob B. U. Haldorsen*, Douglas E. Miller‡, and John J. Walsh**

ABSTRACT

We describe a method for extracting and deconvolving a signal generated by a drill bit and collected by an array of surface geophones. The drill-noise signature is reduced to an effective impulse by means of a multi-channel Wiener deconvolution technique, producing a walk-away reverse vertical seismic profile (VSP) sampled almost continuously in depth. We show how the multichannel technique accounts for noise and for internal drill-string reflections, automatically limiting the deconvolved data to frequencies containing significant energy.

We have acquired and processed a data set from a well in Germany while drilling at a depth of almost 4000 m. The subsurface image derived from these data compares well with corresponding images from a 3-D surface seismic survey, a zero-offset VSP survey, and a walk-away VSP survey acquired using conventional wireline techniques. The effective bandwidth of the deconvolved drill-noise data is comparable to the bandwidth of surface seismic data but significantly smaller than what can be achieved with wireline VSP techniques.

Although the processing algorithm does not require the use of sensors mounted on the drill string, these sensors provide a very economic way to compress the data. The sensors on the drill string were also used for accurate timing of the deconvolved drill-noise data.

INTRODUCTION

If he can use the energy released by a working bit to make real-time images of the rock formation ahead of the bit a driller may be able to avoid some expensive and at times catastrophic surprises. The usefulness of drilling noise as a seismic source depends on the signal bandwidth, on how well one can estimate the seismic signature of the radiated

energy, and also on the strength and spectral content of the noise around the working rig. If viable, the drill-noise seismic source may also be used to acquire more cost-effective 3-D, reverse vertical seismic profile (VSP) data.

Typical algorithms used to obtain subsurface images from seismic data (Miller et al., 1987) assume that input data represent the earth response to a purely impulsive source. For physical sources, a preprocessing deconvolution is required to remove the effect of the source signature and to produce an estimate of the earth impulse response. If the source has an extended signature, knowledge of this signature is required for the deconvolution.

To use the drill bit as a seismic source, we must convert the continuous, chaotic signal generated at the bit to an equivalent impulse. Previously published work in this area relies on measurements by accelerometers on the drill string to provide an estimate of the seismic signature of the drill bit (Staron et al., 1985; Rector et al., 1988; Rector, 1990; Rector and Marion, 1991; Rector and Hardage, 1992). From this estimate they derive an inverse filter that they apply to reduce the data to an estimate of the earth impulse response. To obtain a good estimate of the drill-bit signature from these accelerometers, one first has to remove the drill-string transfer function and unrelated noise from the accelerometer measurement.

In contrast, the method that we are proposing makes essential use of the focusing capability of a large array of surface geophones both to obtain the drill-bit signature and to provide an optimal, multichannel deconvolution filter. While a rig accelerometer can be used for initial data compression by crosscorrelation and stacking and for establishing a time reference, there is no need for accelerometer data in designing the deconvolution operator. This operator is found from a least-squares minimization procedure using the geophone array as described in Haldorsen et al. (1992a), Miller et al. (1990), and Haldorsen et al. (1992b). The optimal inverse and its application to conventional VSP data are described in Haldorsen et al. (1994).

Manuscript received by the Editor July 19, 1993; revised manuscript received September 9, 1994.

*formerly Geco-Prakla, Bucholzerstrasse 100, D 30655 Hannover, Germany; presently Schlumberger-Doll Research, Old Quarry Road, Ridgefield, CT 06877-4108.

‡Schlumberger-Doll Research, Old Quarry Road, Ridgefield, CT 06877-4108.

**Schlumberger Well Services, 1325 S. Dairy Ashford, Suite 350, Houston, TX 77077.

© 1995 Society of Exploration Geophysicists. All rights reserved.

The geophone array gives a laterally extended image of the formation ahead of the drill bit. If provided in or close to real time, such an image could provide timely information for the drilling operation.

We will start by giving a short description of the algorithm. The use of accelerometers for timing reference is described in the main body of the text and modified for correlated data in Appendix A.

We will show results from a recent research experiment. The well is owned by a consortium of German oil companies and operated by RWE-DEA. The images obtained from the drill-noise data will be compared to the images obtained from conventional seismic data.

PROCESSING ALGORITHM

We use four basic processing steps in transforming the drill-noise data to an image of the formation.

- 1) Apply focusing analysis to find the velocity that focuses most of the energy on the location of the drill bit. This velocity gives a first estimate of the moveout times.
- 2) Design and apply a uniform deconvolution filter that best spikes the moveout-corrected traces.
- 3) Correct the moveout times by picking break times on the deconvolved data, then repeat the previous step.
- 4) Make an image from the deconvolved traces using the generalized Radon transform (GRT) migration algorithm described in Miller et al. (1987).

By comparing the measurements by the geophones and the accelerometers on the drill string, we can fix the vertical propagation time in the formation to aid in building the migration velocity model.

The algorithm used for signature estimation and inverse filtering was described in Haldorsen et al. (1994). The following summary gives the formulas essential to the drill-noise application. In addition, we describe the semblance analysis used to find the initial time delays and how we use the accelerometers for calibrating the vertical propagation time.

The same symbol is used to describe a function both in the time and frequency domains, and we do not distinguish notationally between a parameter and its estimate.

Source signature

Each trace s_n is thought of as a superposition of a common signal f , delayed by the propagation time t_n between the drill bit and the n th receiver, and a variable "noise" \mathcal{N}_n . In the frequency domain, the trace model is written as

$$s_n(\omega) = f(\omega)e^{i\omega t_n} + \mathcal{N}_n(\omega). \quad (1)$$

\mathcal{N}_n includes the reflected field, but for the case of drill-bit data, is dominated by undesired energy. One of the objectives for the deconvolution filter is to attenuate this undesired energy.

Provided that the noise is spatially zero-mean, i.e.,

$$\frac{1}{N} \sum_{n=1}^N \mathcal{N}_n(t + t_n) = 0, \quad (2)$$

an unbiased estimate of f is given by

$$f(\omega) = \frac{1}{N} \sum_{n=1}^N s_n(\omega)e^{-i\omega t_n}. \quad (3)$$

Without a direct recording at the source, we have no absolute measure of t_n . We therefore split t_n into a vertical propagation time t_0 to an (imagined) receiver vertically above the drill bit and a time lag Δt_n , relative to t_0

$$\Delta t_n = t_n - t_0. \quad (4)$$

A delayed estimate of f is then given by

$$\begin{aligned} f_1(\omega) &= f(\omega)D_0(\omega) \\ &= \frac{1}{N} \sum_{n=1}^N s_n(\omega)e^{-i\omega\Delta t_n}, \end{aligned} \quad (5)$$

where the operator

$$D_0(\omega) = e^{i\omega t_0} \quad (6)$$

imposes a delay by t_0 . D_0 defines the time reference and is found by comparing the estimate f_1 , using equation (5), with an independent estimate from accelerometers on the drill string.

Deconvolution filter

An inherently stable inverse filter F that attempts to spike the signature estimate f_1 at the same time that it minimizes the average filtered noise $1/N \sum_n F(\omega)\mathcal{N}_n(\omega)$ can be conveniently written as

$$F(\omega) = \frac{f_1^*(\omega)}{|f_1(\omega)|^2} S(\omega)D_0(\omega). \quad (7)$$

We use * for "complex conjugate." $S(\omega)$ is the frequency-domain semblance, defined as the ratio between the coherent and total energy averaged across the array

$$S(\omega) = \frac{|f_1(\omega)|^2}{E_T(\omega)}, \quad (8)$$

and E_T is the average total energy of the raw traces

$$E_T(\omega) = \frac{1}{N} \sum_{n=1}^N |s_n(\omega)|^2. \quad (9)$$

In equation (7), the first factor $f_1^*(\omega)/|f_1(\omega)|^2$ is recognized as a conventional spiking deconvolution filter with $S(\omega)$ acting as a band-limiting weighting term passing frequencies where the signal energy is higher and attenuating frequencies where the signal energy is lower compared to the noise. The reflected field is spectrally coherent with f and will not be attenuated by F , provided the array is large enough that the reflected signal satisfies condition (2).

Initial time delays from semblance analysis

We use semblance analysis with a homogeneous, isotropic earth model to find initial estimates of the relative time

delays Δt_n . The initial estimates are refined by subsequent iterative repicking on deconvolved data, thereby minimizing the impact of the initial, oversimplified earth model.

From equations (7) and (5) we see that the semblance is equal to the filtered signal amplitude

$$S(\omega) = F(\omega)f(\omega), \tag{10}$$

a real valued number. The peak amplitude in the time domain of the filtered signature is thus equal to the frequency-averaged semblance S_0 defined by

$$S_0 = \frac{1}{N_\omega} \sum_{\omega} S(\omega). \tag{11}$$

N_ω is number of frequency samples used in the calculation.

For a homogeneous isotropic medium, we can parameterize the relative time delays Δt_n in terms of the acquisition geometry and the acoustic velocity c as

$$\Delta t_n = \frac{1}{c} (|\mathbf{r}_n - \mathbf{r}_s| - |\mathbf{r}_0 - \mathbf{r}_s|), \tag{12}$$

where \mathbf{r}_s is the position of the drill bit, \mathbf{r}_0 the position of a (imagined) zero-offset receiver, and \mathbf{r}_n the position of the receiver n .

Using equations (11), (8), (5), (3), and (12), we get the following parameterization of the frequency-averaged semblance S_0

$$S_0(c, \mathbf{r}_s) = \frac{1}{N_\omega} \sum_{\omega} \frac{\left| \frac{1}{N} \sum_{n=1}^N s_n(\omega) e^{-i\omega/c |\mathbf{r}_n - \mathbf{r}_s|} \right|^2}{E_T(\omega)}. \tag{13}$$

The value of c that maximizes S_0 also gives maximum peak amplitude for the deconvolved signal. We use this value of c in equation (12) to find initial estimates of Δt_n .

Reference time

The deconvolution operator (7) includes an undetermined time-shift operator D_0 , defined by equation (6). D_0 can be determined by applying the deconvolution filter to an estimate of the drill-bit signature independently obtained from an accelerometer mounted on the top of the drill string. The analysis runs as follows.

An accelerometer at the drill string measures

$$s_a(\omega) = T(\omega)f_b(\omega)e^{i\omega t_s}, \tag{14}$$

where the signal f_b generated by the drill bit is delayed by the propagation time t_s for an extensional wave along the drill string (Rector and Marion, 1991). T is the accelerometer response to the disturbance by a unit spike at the drill bit at time $t = -t_s$: the drill-string transmission response with the time delay t_s in the drill string removed.

In equation (14), we have two equations (complexs,) with five unknowns (t , and complex T and f_b). Assuming that T is minimum-phase and $|f_b(\omega)|^2 = 1$, we can estimate T using standard techniques. Then, by eliminating T from s_a we get the following estimate of $f_2(\omega) = f_b(\omega)e^{i\omega t_s}$

$$f_2(\omega) = \frac{T^*(\omega)}{|T(\omega)|^2} s_a(\omega). \tag{15}$$

It follows from expressions (7), (6), and (5) that $F(\omega) = f^*(\omega)/E_T(\omega) D_0(\omega)e^{-i\omega t_0}$ and we see that the application of F to the accelerometer-derived signature f_2 gives the relation

$$F(\omega) \frac{T^*(\omega)}{|T(\omega)|^2} s_a(\omega) = F(\omega)f_2(\omega) = \frac{f^*(\omega)f_b(\omega)}{E_T(\omega)} D_0(\omega)e^{i\omega(t_s - t_0)}. \tag{16}$$

The right-hand side of this equation represents a correlation function between f and f_b , shifted in time by the operators D_0 and $e^{i\omega(t_s - t_0)}$. In the time domain, the peak of this correlation function should fall at the propagation time t_s in the drill string. Propagation time t_s can be found by analyzing $T(t)$ —or from a priori knowledge of the propagation speed of extensional waves in the drill string. Thus, D_0 can be obtained from equation (17) as the operator that shifts the peak of the correlation function in equation (17) to $t = t_s$.

It is important to realize that f and f_b are not equal. Here, f is a measure of the seismic signal emitted at the drill bit and will include signal radiated both directly as well as energy radiating from the drill bit after first having been reflected internally in the drill string. The signature f_b is a measure of only the primary drill-bit signature. Provided both are well estimated, f is related to f_b by

$$f(\omega) = R(\omega)f_b(\omega), \tag{17}$$

where R is the reflection response of the drill string including signal radiated directly as well as after internal reflections in the drill string.

Relative signal energy and effective bandwidth

Table 1 relates signal and total energies in raw and deconvolved data to the semblance S and the average total energy E_T . The semblance at any given frequency, as the ratio between the signal energy and the average total energy, is not affected by the deconvolution. Deconvolution changes the average total energy from E_T to S , the signal energy from SE_T to S^2 , leaving their ratio unchanged. On the other hand,

Table 1. Absolute **and** relative signal energies before and after deconvolution.

	Before deconvolution	After deconvolution
Total energy	$E_T(\omega)$	$S(\omega)$
Signal energy	$S(\omega)E_T(\omega)$	$S(\omega)S(\omega)$
	$\sum_{\omega} S(\omega)E_T(\omega)$	$\sum_{\omega} S(\omega)S(\omega)$
Signal-to-total energy	$\frac{\sum_{\omega} S(\omega)E_T(\omega)}{\sum_{\omega} E_T(\omega)}$	$\frac{\sum_{\omega} S(\omega)S(\omega)}{\sum_{\omega} S(\omega)}$

the *overall* relative signal energy may be changed. This can be thought of as a weighted average of the semblance. The deconvolution changes the weights from E_T to S , thereby changing the emphasis from frequencies with high energy to frequencies with high semblance. If the difference in the spectra of E_T and S is large, there will be a significant change in the relative signal energy.

In the following section, we will use the “effective bandwidth” introduced by (Haldorsen et al., 1994) to quantify and compare wireline and drill-noise data. The effective bandwidth of the deconvolved data is equal to the width of a square-box semblance spectrum that would yield the same relative signal energy. The effective bandwidth is measured by:

$$\Delta\Omega_{eff} = \frac{S_0}{\alpha_{S/T}} \Omega, \quad (18)$$

where $\alpha_{S/T}$ is the relative signal energy after deconvolution calculated over the frequency range Ω . S_0 is the frequency-averaged semblance given by equation (11).

APPLICATION

Drill-noise data were acquired while drilling through limestone and salt at a depth of about 3740 m. The well was operated by RWE-DEA and owned by RWE-DEA, BEB, Mobil, Preussag, and WIAG. Figure 1 shows a plan view of the acquisition geometry. The geophone array consisted of one north-south line and five east-west lines each 1950 m long. The north-south line extended from 625 m to the south of the rig to 1325 m to the north. The five east-west lines were parallel with 50 m separation, intersecting the north-south line about 700 m to the north of the rig. Each line consisted of 40 groups of 24 vertical geophones. The distance between the centers of the groups was 50 m, and 2 m between individual geophones. The wellhead was the main source of noise and the groups were directed along straight lines pointing toward the wellhead to attenuate the surface noise spreading out from there. In addition to the geophones, data were recorded from two accelerometers mounted on the top of the drill string.

A schematic of the bottom hole assembly (BHA) is shown in Figure 2. The changes in the cross-section of the drill string may be accompanied by a change in acoustic impedance for extensional waves in the drill-string of up to a factor 3.

Figure 3 shows a 4 s subrecord of raw data. The rig is located about 300 m away from the center of this line. The average signal semblance in the raw data in Figure 3 is less than 2×10^{-4} . At these low levels, it is all but impossible to find the signal. To get a reasonable ratio of signal-to-noise energy in the deconvolved traces, we needed to acquire data over as much as 5 hours of drilling. The geophone traces were correlated and stacked using the drill-string accelerometers as a reference signal. The correlation and stacking meant a very significant saving in data-storage requirements, compressing the 5 hours of waveforms into one single 6 s record, a saving by a factor of 3000. Whereas the full-waveform data would require almost 9 Gbytes of storage space, the correlated and stacked record required only 3 Mbytes. The use of correlated data as input makes it

necessary to change the processing algorithm slightly. These modifications are discussed in Appendix A.

When the optimal deconvolution algorithm is applied to data with a low relative signal energy, the bias of the deconvolved data by the autocorrelations of the input traces may become significant. The modifications necessary to avoid these contributions are discussed in Appendix B. In the applications that follow, we have removed the autocorrelation bias.

In Figure 4 we show geophone data after reference correlation from one of the east-west lines and in Figure 5 from the north-south line. The sections comprise the 5 hours of raw data, corresponding to 5 m of rock drilled. The correlated data are dominated by low frequency waves with a conical space-time structure (either surface waves or head waves (Rector and Hardage, 1992) generated in the borehole or at the surface). The dispersive hyperbolic events after about 2.5 s in Figure 4a and at all the near traces in Figure 5 are up to two orders of magnitude higher amplitude than the rest and have been clipped for display. They originate at the rig and have a propagation velocity of around 340 m/s, consistent with air-coupled surface waves. Looking at a section from 0.2 to 1.2 s of data in Figure 4b, the direct body waves are clearly visible at around 0.4 s. The high-amplitude hyperbolic event between 0.7 and 0.9 s is a conical wave that

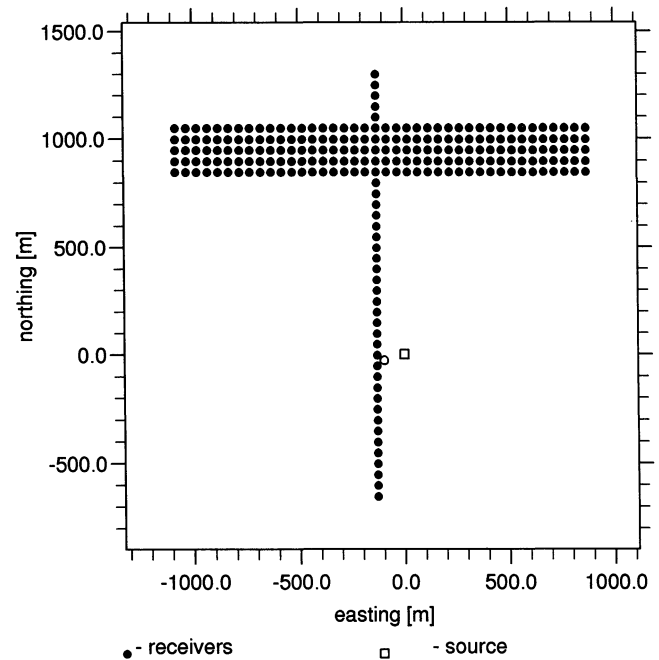


FIG. 1. Top view of acquisition geometry used for the drill-noise data. The drill bit (marked with \square) was at the coordinates (0, 0) at the surface and at a depth of 3740 m. The rig (marked with \circ) was 100 m to the west and 50 m to the south of the rejection of the bit on the surface. The geophone array marked with \bullet consisted of one north-south line and five east-west lines each 1950 m long. The north-south line extended from 625 m to the south of the rig to 1325 m to the north. The five east-west lines were parallel with 50 m separation, intersecting the north-south line about 800 m to the north of the rig. The 2-km long lines each contained 40 receivers at 50 m intervals.

probably also originates at the rig. This wave has a horizontal propagation velocity of about 1500 m/s.

Effectively free from random noise, the correlated and stacked data in Figure 4 are dominated by the components of the geophone noise that correlate well with the accelerometer trace. Much of this noise energy may be caused by surface sources such as pumps and generators, unrelated to the seismic signal generated at the drill-bit. The objective of the array-based optimal deconvolution will be to attenuate this noise, and at the same time, to further concentrate the drill-bit signal.

Figure 6 shows the power spectrum in a logarithmic scale between 0 and -60 dB of the average total energy E_T for the correlated data in Figure 4. The data are extremely narrow-band with most of the energy falling between 6 and 10 Hz; the power is down about 15 dB from its maximum by 14 Hz and another 20 dB by 18 Hz. Between 30 and 40 Hz, and

above 65 Hz the power falls below -60 dB. The attenuation below 6 Hz is caused by the acquisition filter. The reason for the depression between 30 and 40 Hz is not known. It could be related to the location of the accelerometer as suggested in Rector (1990), but could, at least partly, be features of the drill-bit signature and the transmission response of the drill string. We will see in the next section that the optimal array deconvolution closes this gap almost entirely. This is an indication that the signal-to-noise level is constant through the notch and appears to support the contention of Rector (1990).

Deconvolution

The optimal deconvolution will replace the spectrum of the signal measured directly from the raw traces by the semblance spectrum associated with the applied time delays t_n across the array of geophones [equation (10)]. We obtain our initial estimates of relative time delays from a semblance analysis using the simplified parameterization (13). The final time delays are found by an iterative deconvolution and repicking.

Figure 7 shows a map of the semblance S_0 as a function of velocity c and source depth r_s . The map is derived from 200 traces from the five east-west lines. The plot shows a high ridge along a curve where the product of velocity and source depth is roughly constant. This interdependency means that we cannot simultaneously determine both these parameters. At the nominal drill-bit depth of 3740 m the maximum average semblance of 0.01 corresponds to a value of 3440 m/s for c . Using the relative time delays from equation (12) as initial values, deconvolution and automatic repicking of times were iterated until the average signal energy in the deconvolved data converged to a constant value.

Figures 8 and 9 show the results of applying the array-based, optimal deconvolution operator to the data. Except for the zero-time reference, the data are comparable to Figures 4 and 5. We see a clear improvement over the field-correlated data in the definition of the direct signal. The surface waves dominating Figure 4 are strongly attenuated, indicating that they are spectrally different from our estimate of the drill-bit signal. The spectral separation between signal and noise is sensed by the deconvolution algorithm and used in the semblance weights in equation (7) for an optimal noise suppression.

The data of Figure 4 could be improved by applying additional, interactively designed band-pass and deconvolution filters (Rector and Marion, 1991). The filter (7) attains the "best possible" result (in a least-squares sense) automatically and without the subjective and labor intensive step of selecting filter parameters (Haldorsen et al., 1994).

In Figure 9, the direct arrivals can be traced to about 300 m from the rig (by trace 17 on the plots). Unveiled by the attenuation of the different surface-related wavetrains, an early arrival has appeared, preceding the direct drill-bit arrival by about 0.070 s. The arrival time and the higher curvature of this head wave indicate that it originates some distance above the drill bit. Similar waves are observed by Rector and Hardage (1992). The fact that the head wave has been enhanced by the optimal deconvolution means that it is spectrally similar to the direct arrivals, and that it is sepa-

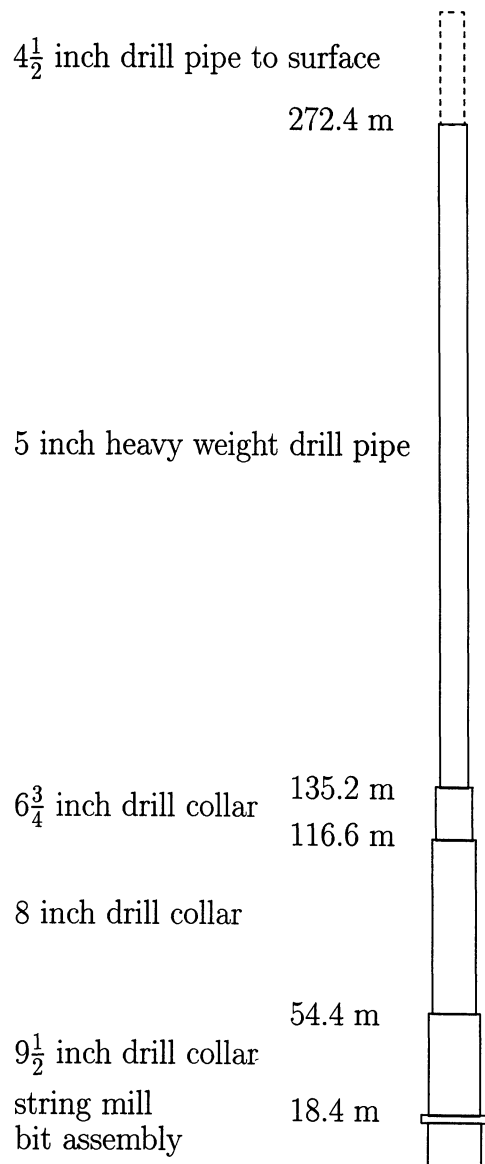


FIG. 2. Schematic section of the bottom hole assembly (BHA). The cross-sectional changes represent acoustic impedance changes of up to a factor of 3.

rated from the direct arrivals in the deconvolved data means that it has a space-time relationship that is sufficiently different for it not to be focused with the direct arrivals.

The power spectrum $|f(\omega)|^2$ of the estimated signature, shown in Figure 10, does not drop off quite as much with frequency as the average total energy E_T . The power at 30 and 50 Hz is about 15 dB higher than for E_T and the trough around 35 Hz is not quite as deep. The amplitude spectrum of the deconvolved signature $F(\omega)$ $f(\omega)$ is equal to the semblance $S(\omega)$, shown in Figure 11. S is the ratio of $|f(\omega)|^2$, from Figure 10, to $E_T(\omega)$ from Figure 6. This means that the spectral energy of the deconvolved signal will increase when the decrease in $|f(\omega)|^2$ is less than in $E_T(\omega)$. For this reason we see an increase in the semblance at frequencies from 6 to 35 Hz (Figure 11). Although not flat, the semblance is broad-banded with most of its energy between 20 and 70 Hz. The semblance spectrum has significant troughs at around 35, 55, and 63 Hz.

It is argued in (Rector, 1990) that the deep spectral trough between 30 and 40 Hz observed in the correlated data comes from the reference accelerometer and is not a feature of the drill-bit signal but is related to the location of the reference accelerometer on the swivel. For his reference accelerometer, this trough was partly filled with noise generated by a "rocking motion" of the swivel around the pin connecting the swivel to the bail. By using a second, horizontal accelerometer, he was able to adaptively model and remove this noise from the reference signal. In our experiment, we have attempted to minimize the contamination of the reference signal by carefully selecting the location of the accelerometers. Moreover, if the noise described in Rector (1990) was to be picked up by the reference accelerometers, the noise would appear to be incoherent in the correlated geophone traces and therefore be attenuated by the optimal deconvolution filter. Although showing some fluctuations, the rela-

tive flatness of the semblance spectrum in Figure 11 indicates that the correlated data have relatively little variation in signal-to-noise ratio in the region of the spectral trough.

Time calibration

Figure 12 shows the drill-string transmission response $T(t')$ derived from the accelerometer trace assuming T is minimum phase and the spectrum of the drill-bit signature is white as discussed in the section on reference time. The time $t' = t + t_s$ is referred to the time of emission at the drill bit, which is $t_s = 0.78$ s before the signal is recorded by the accelerometer. The peak breaking 1.45 s later (at $t' = 2.22$ s) is consistent with a reflection from the top of the BHA, 272 m above the drill bit (Figure 2). This reflection confirms that the propagation speed of sound in the drill string is 4780 m/s, practically identical to the value 4760 m/s found in Rector and Marion (1991).

Figure 13 shows the result of filtering the correlated accelerometer trace by the array-based deconvolution filter with and without the additional filter $T^*(\omega)/|T(\omega)|^2$, prescribed by equation (A-11), Appendix A. The clear peak at about 0.78 s indicates that the correlation is good between the signature f_2 , as estimated from the accelerometer, and the signature f_1 , radiated into the formation at the drill bit and estimated by the focused geophone array. The extra filter removes the ringing associated with the drill-string response and also shifts the maximum of the envelope of the correlation. This shift is caused by the minimum-phase nature of the drill-string response. The asymmetry of the correlation function indicates that the two signatures are different. This should be expected as the radiated signature includes energy multiply reflected in the drill string.

The deconvolved data shown in Figures 8 and 9 were shifted in time to let the maximum of the filtered

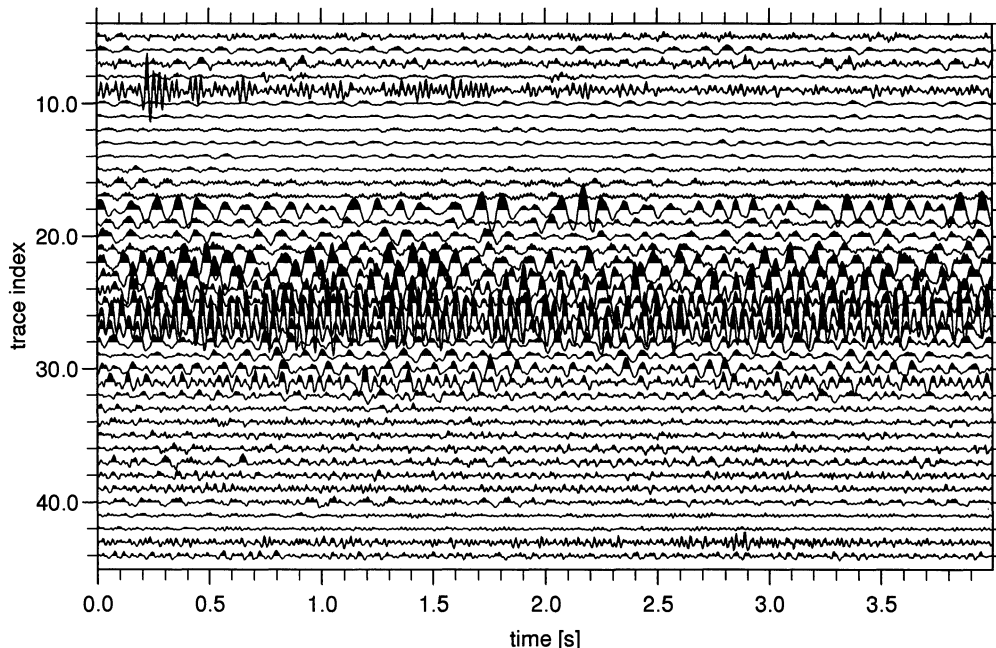


FIG. 3. A 4 s subrecord of raw drill-noise data. The rig site is located about 300 m away from the center of the line.

accelerometer trace fall at time $t_s = 0.782$ s, the estimated propagation time through the drill string.

DISCUSSION

The drill-bit source can be characterized by its bandwidth and also by comparison to data acquired using other sources and acquisition techniques. To compare the seismic images we obtained from the drill-noise data, we had access to good quality seismic data including a 3-D surface seismic data set, a zero-offset VSP, and an 8-level walk-away VSP. Both the VSP and the walk-away VSP were designed to cover the same depth range as the drill-noise data.

Support data

Surface seismic data of 48-fold were acquired with vibrators at 50 m source interval and 25 m receiver interval. The geophone groups consisted of patterns of 24 vertical geophones and the source of a stack of eight 8 s, 10-80 Hz sweeps by three vibrators. The image obtained along a north-south line through the wellhead is shown in Figure 14. The imaging was done using the GRT algorithm described in Miller et al. (1987). The target for the well was below the prominent reflectors at about 2.7-2.8 s. In obtaining the image, the assumption is made that the formation is flat in

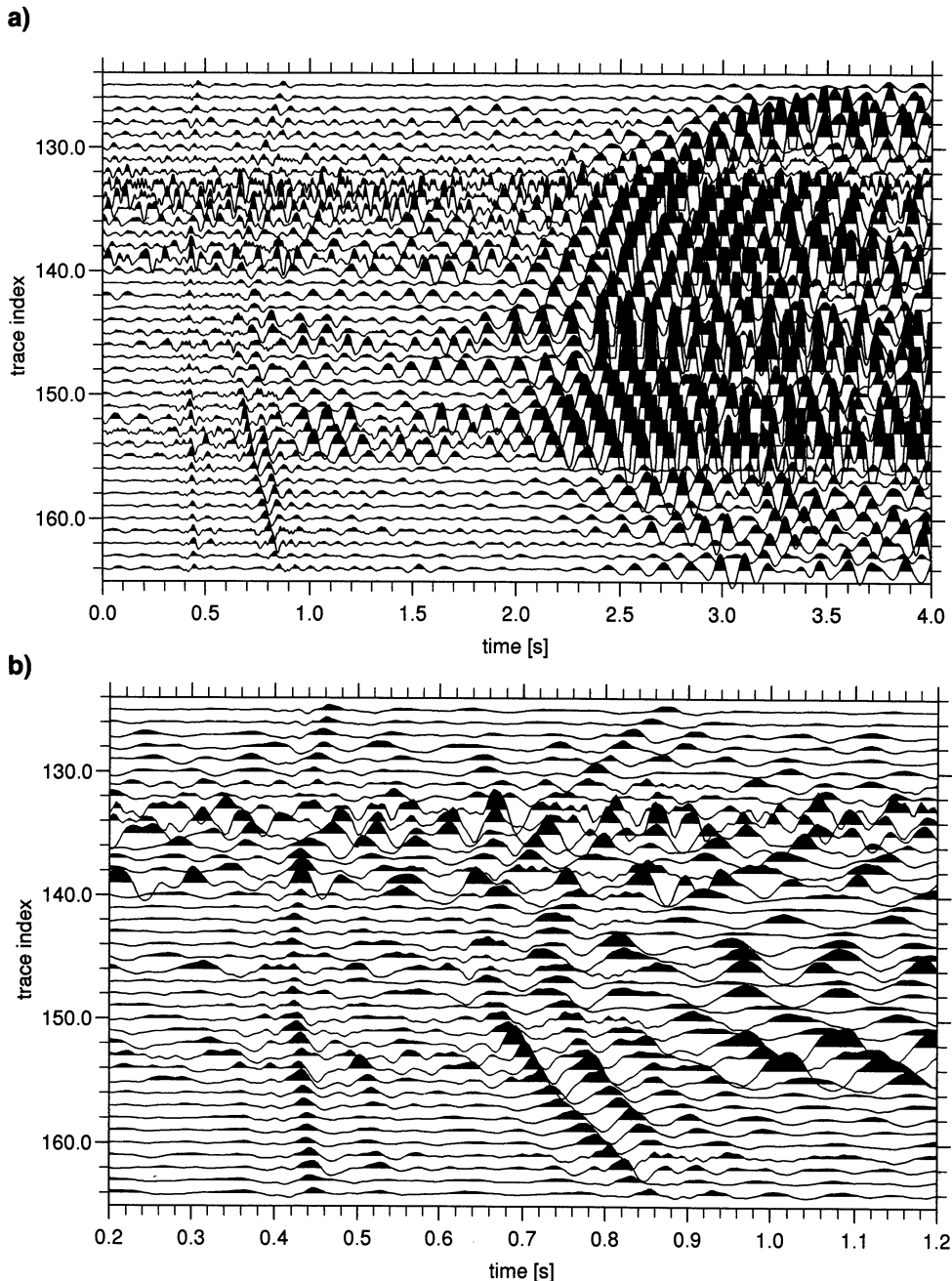


FIG. 4. Geophone data of (a) 4 s and (b) 1 s lengths from one of the east-west lines after correlation with the signals recorded by accelerometers mounted on top of the drill string. The section shown comprises 5 hours of raw data. The slow, high-amplitude events at times later than 2.5 s have been clipped for the display.

the crossline east-west direction. This assumption enables us to use all six lines in forming the image.

The zero-offset VSP was recorded with a Schlumberger SAT* Seismic Acquisition Tool over depths ranging from 3500 to 3850 m using dynamite charges in a 20-m deep hole approximately 100 m from the wellhead. In Figure 15, we show the “look-ahead” VSP image (Haldorsen et al., 1994) together with a bordering section surface seismic image. The data have been deconvolved using essentially the same processing algorithm as described in this paper, then cor-

rected to seismic two-way times and coherency filtered with a five-trace running average filter. The deepest receiver position corresponds to 2.4 s two-way time.

For the walkaway VSP, we used a surface aperture similar to that of the drill-noise data. The acquisition was done in the cased hole using the Schlumberger DSA* (downhole seismic array) tool with an array of eight magnetically clamped geophones. The shallowest level was at 3525 m, the deepest at 3630 m. The vibroseis source was run along a north-south line from about 600 m to the south to about 2400 m to the north of the well. The deconvolved data (Haldorsen et al., 1994) were migrated using the GRT algorithm. The resulting

*Mark of Schlumberger

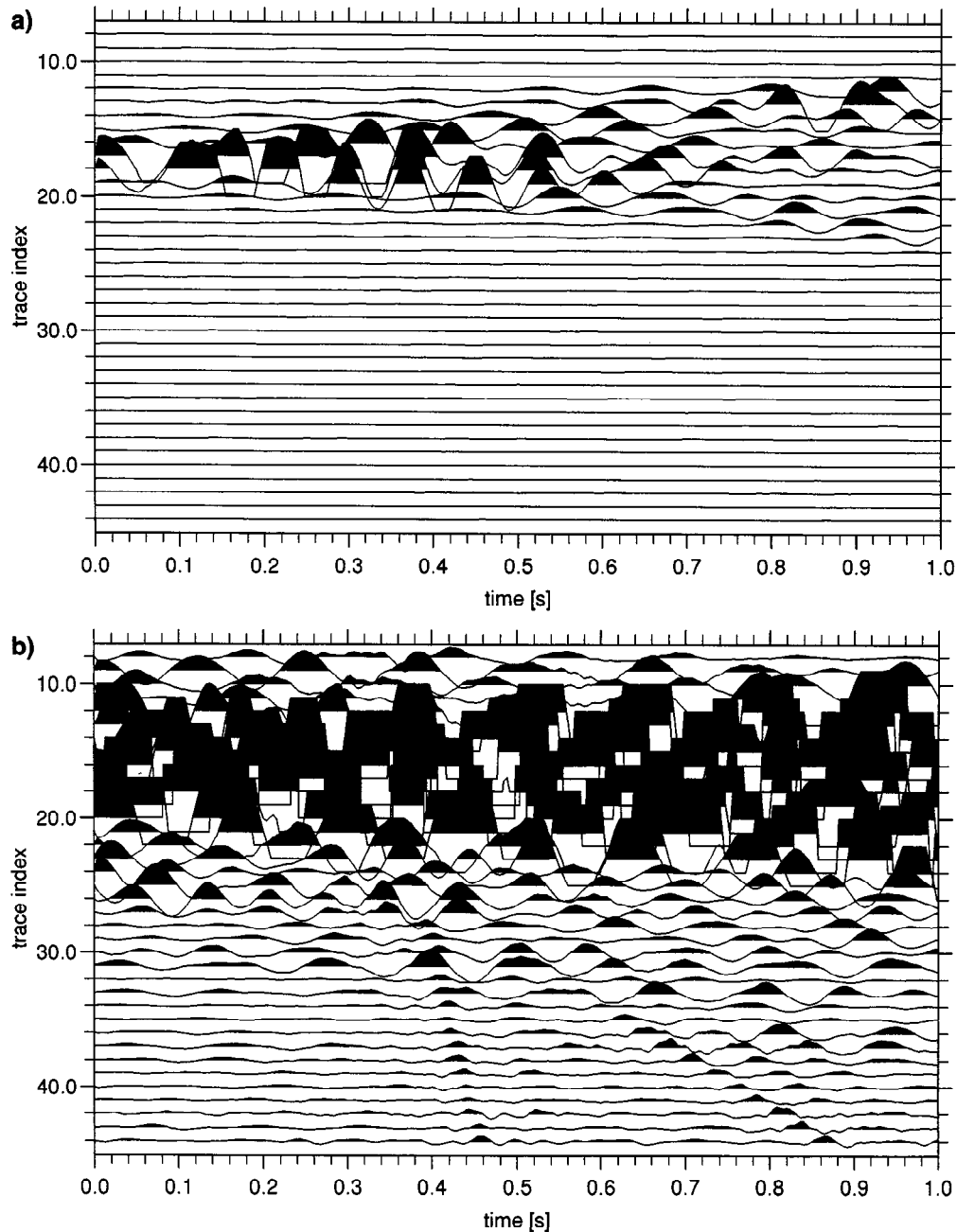


FIG. 5. Geophone data from the north-south line after correlation with the signals recorded by accelerometers mounted on top of the drill string. The traces are plotted in true, relative amplitude and clipped. There is a difference in absolute normalization between plots (a) and (b) of a factor of 40.

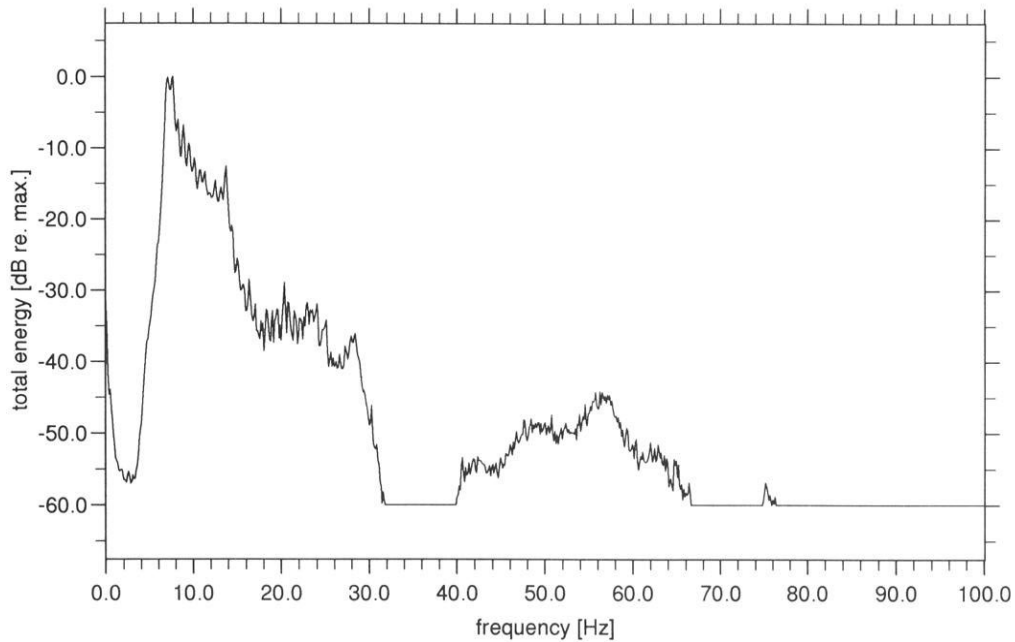


FIG. 6. The average total energy E_T for the correlated data in Figure 4. The spectrum is displayed in a dB scale. The attenuation below 6 Hz is caused by the acquisition filter.

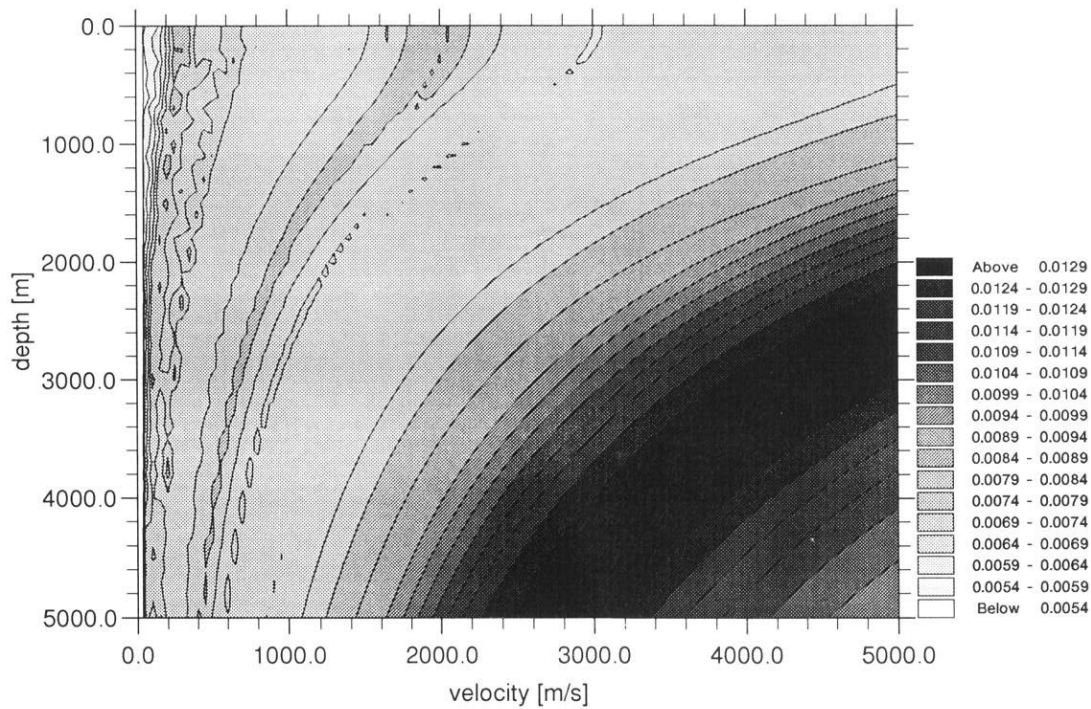


FIG. 7. The semblance function $S_0(c, r_s)$ calculated according to equation (13), with the velocity parameter c running along the horizontal axis and r_s along the vertical axis. The map is coded in scales of grey, with darker colors signifying a larger semblance. Assuming that the drill bit is the most energetic source at a distance from the wellhead equal to the drill-bit depth, we find that the value 3640 m/s for c maximizes the semblance.

image is shown superimposed on the surface seismic image in Figure 16.

It is evident from Figures 14,15, and 16 that the area gives good and consistent seismic data.

Comparison of migrated seismic images

In migrating the drill-noise data, the north-south line was excluded because of a high level of residual noise close to the rig. The seismic image obtained from the five deconvolved east-west lines was projected onto the plane of the north-south

going surface seismic line. The image is shown in Figure 17 at seismic two-way times between 2.4 and 3 s. The image is superimposed on the image from the surface seismic data. The bit depth corresponds to a seismic two-way time of 2.32 s.

The agreement is good between all different sets of images shown in Figures 14, 15, 16, and 17. The reflector seen at about 2.70 s is confirmed by logs. The differences in appearance of this reflector between the different data sets may be caused by both differences in resolution and by differences in geometry.

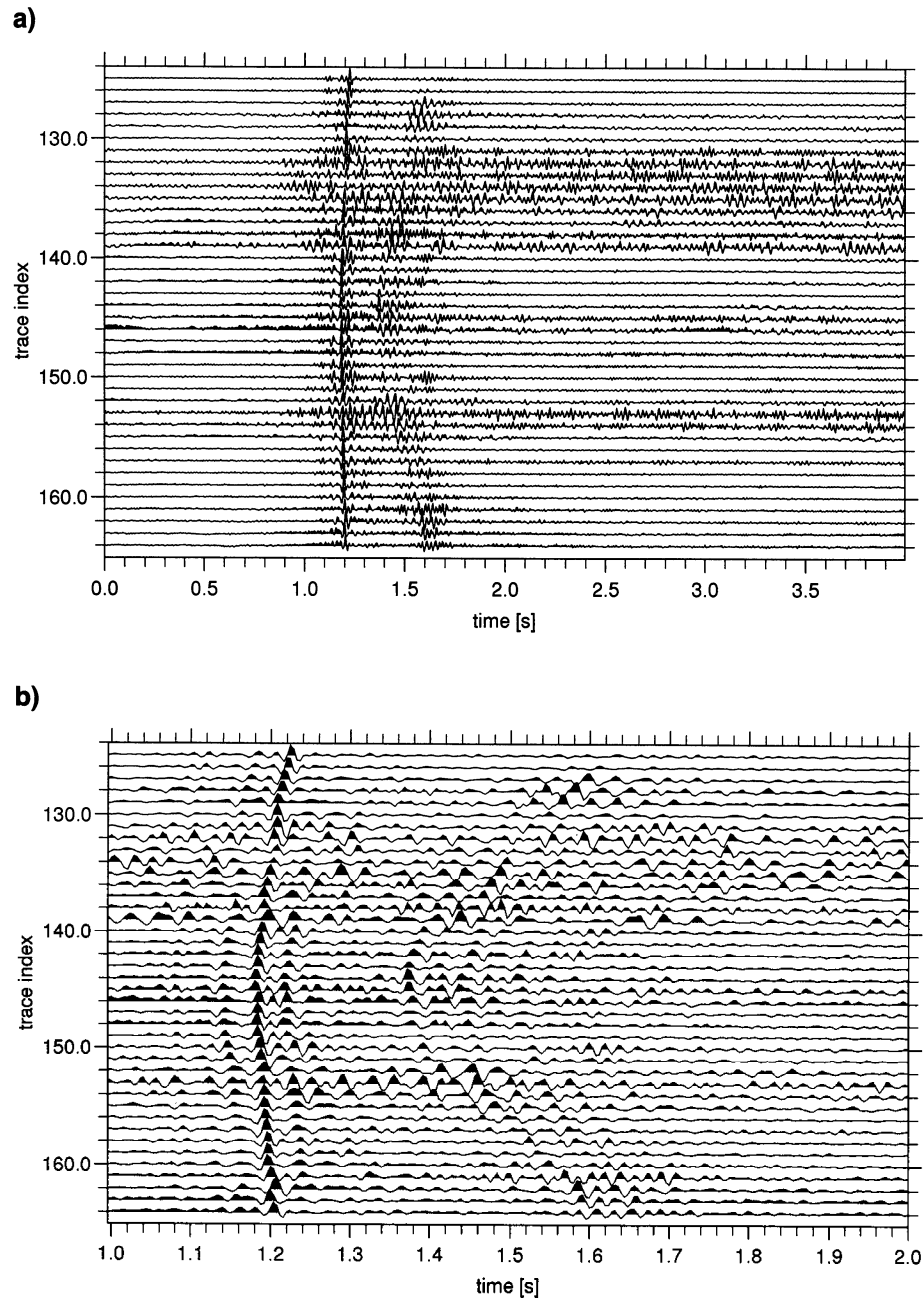


FIG. 8. The same section of the drill-noise data as shown in Figure 4, (a) 4 s and (b) 1 s sections, after applying the optimal deconvolution operator to the data.

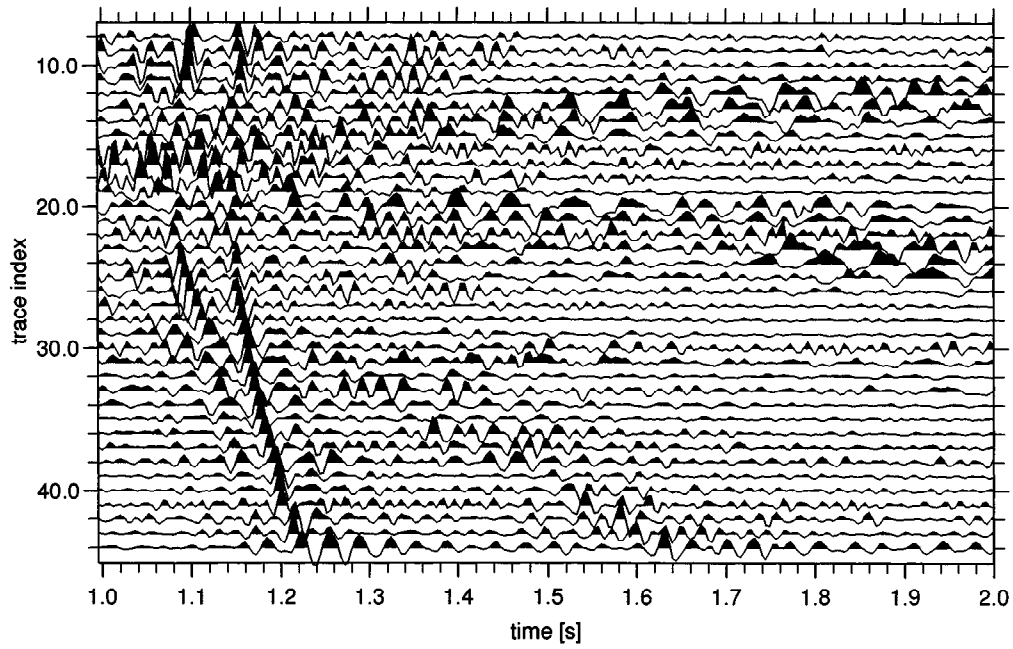


FIG. 9. The same section of the drill-noise data as shown in Figure 5 after applying the optimal deconvolution operator to the data.

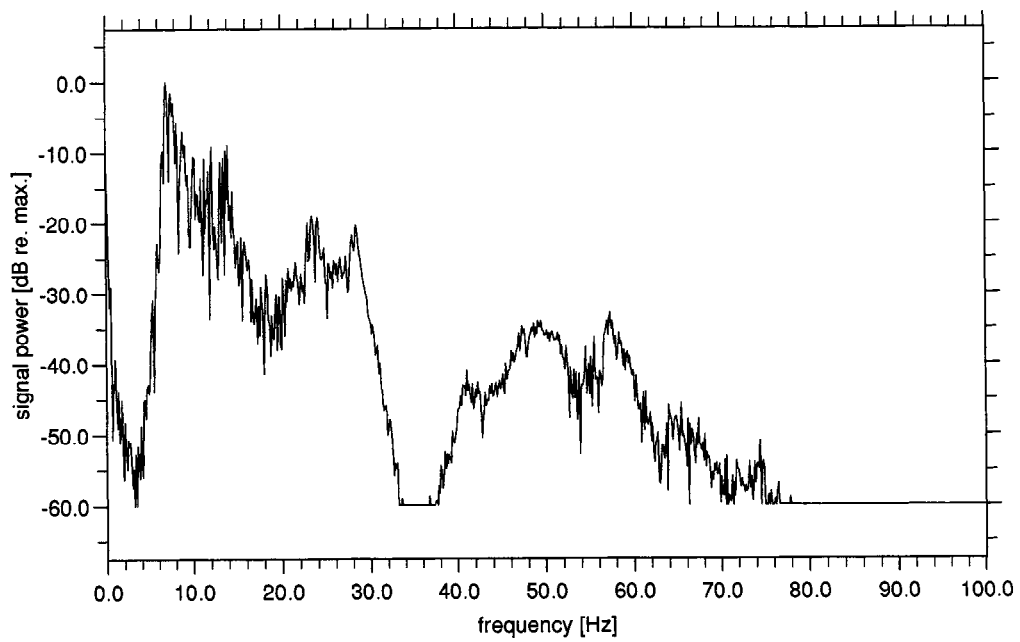


FIG. 10. Amplitude spectrum of estimated signature f . Some higher frequency energy is barely visible between 20 and 30 Hz.

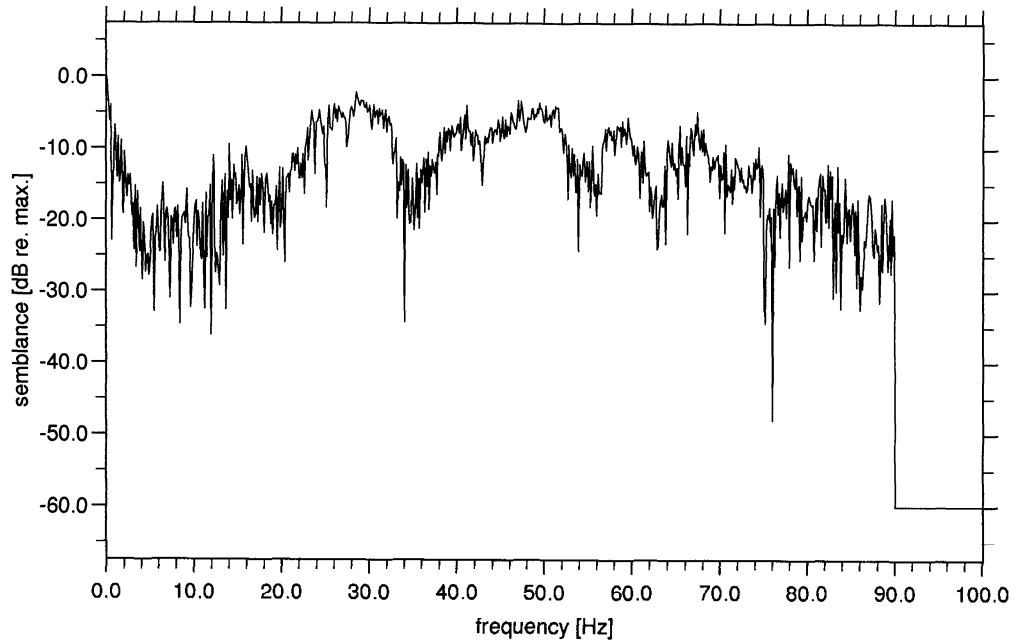


FIG. 11. The semblance spectrum—equal to the amplitude spectrum of the deconvolved signature. Most of its significant energy falls between 20 and 70 Hz with significant troughs around 35, 55, and 63 Hz.

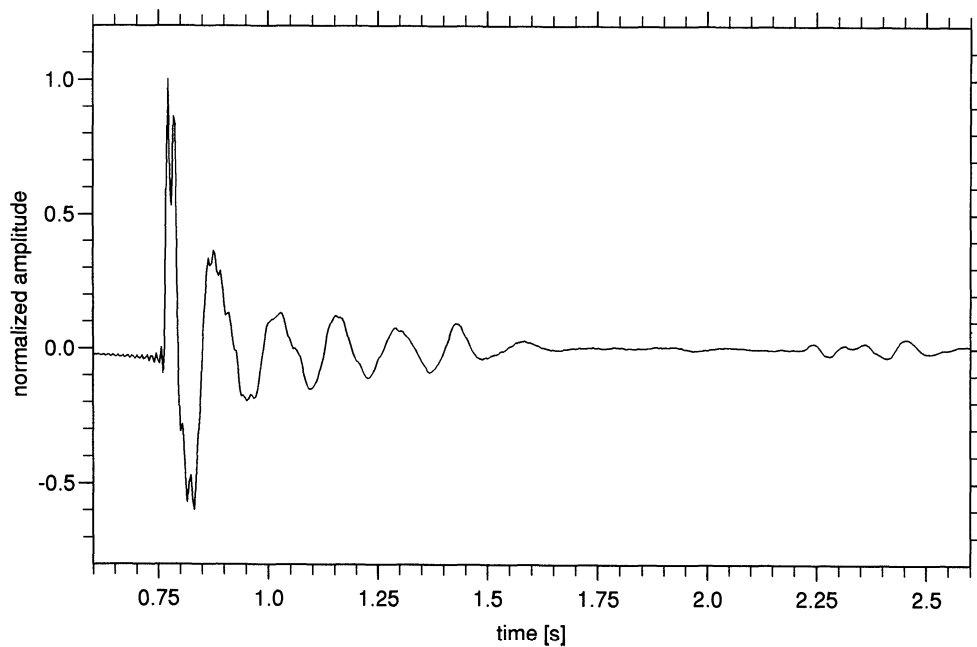


FIG. 12. Drill-string transmission response $T(t')$ derived from the accelerometer trace. The time $t' = t + t_s$ is referred to the time of emission at the drill bit, which is $t_s = 0.78$ s before the signal is recorded by the accelerometer. The peak breaking 1.45 s later (at $t' = 2.22$ s is interpreted as representing the top of the bottom hole assembly (BHA), about 272 m above the drill bit. This reflection confirms that the propagation speed of sound in the drill string is 4780 m/s.

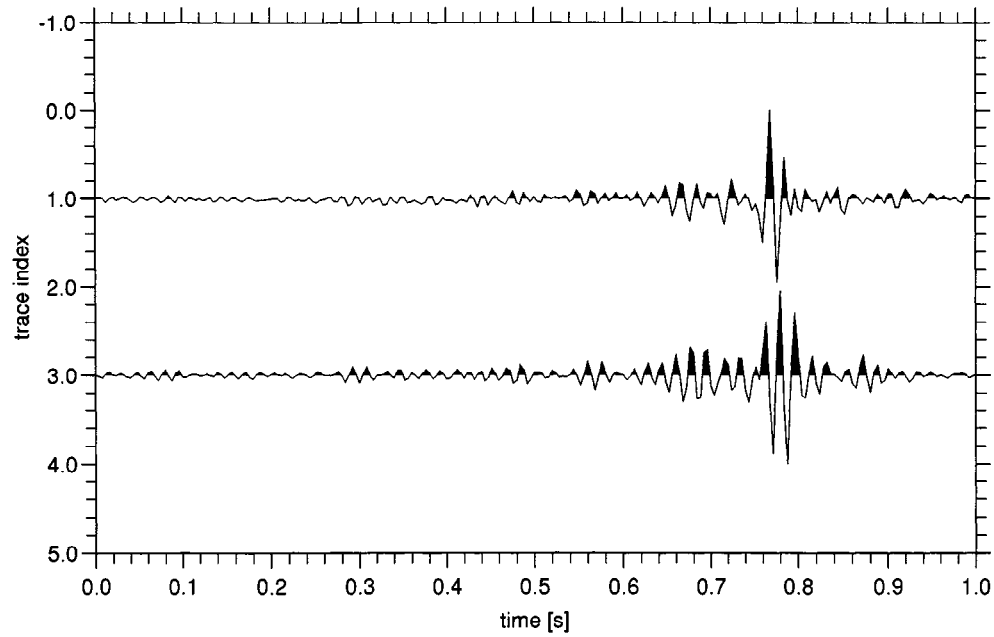


FIG. 13. Deconvolved accelerometer trace: for the top trace (index 1) we applied the complete operator given by the left-hand side of equation (A-11) to the autocorrelated accelerometer trace, and for the bottom trace (index 3) we applied only the deconvolution filter derived from the geophone array.

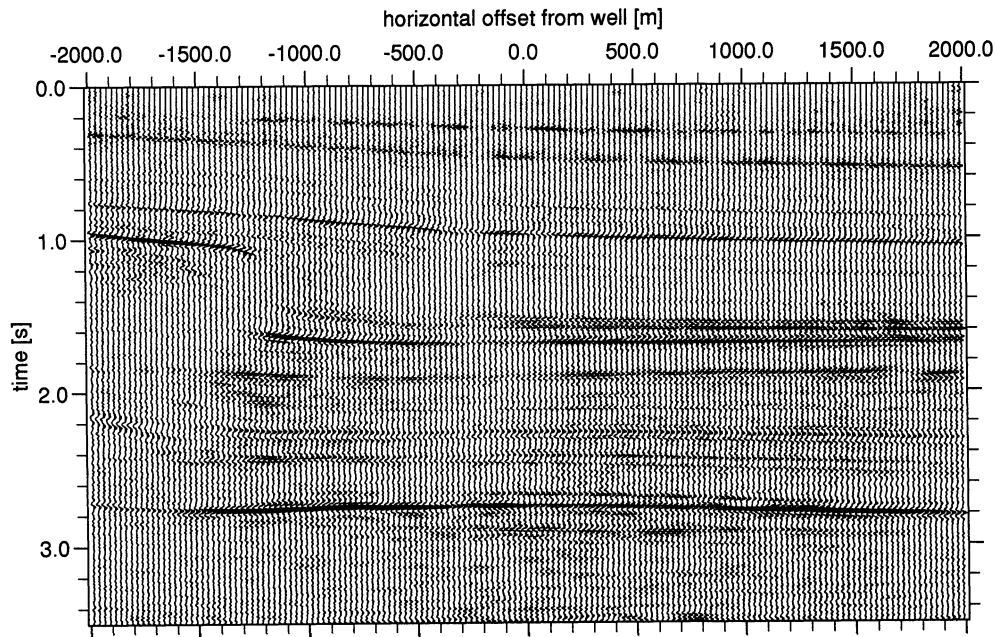


FIG. 14. A time migrated image obtained from the surface seismic data. The line is running from south to north through the wellhead.

To better compare the resolution in the four different seismic data sets we have extracted the traces at the position of the borehole.

Figure 18a shows a comparison of the traces at the position of the well from the four seismic data sets: the surface seismic, the dynamite zero-offset VSP, the wireline vibrator walk-away VSP, and the drill-noise walk-away VSP. The immediate impression from the comparison of the traces is that the two wireline data sets show similar resolution and have better resolution than the surface seismic and the drill-noise seismic data. The surface seismic and the drill-noise seismic data are comparable.

This is confirmed by Figure 18b, showing the spectra of the image traces. The migration process, by transforming from time to "pseudotime" (time converted to depth), smooths the spectrum of the data. The spectrum of the drill-bit seismic image does, however, show residues of the structure evident in Figure 11. The spectrum of the zero-offset VSP is flat over the entire frequency range. The

spectrum of the walk-away data is almost as good. Both the surface and the drill-noise seismic show deficiencies at the higher frequencies.

Comparison of relative signal energies and effective bandwidths

S_0 measures the frequency-averaged ratio of coherent to total energy-in this case the ratio of direct signal to surface wave energies. A value of S_0 of 0.01 for the correlated, stacked, and truncated data means that, on the average, there is 100 times more energy at a given frequency in the surface waves than in the direct signal. Although the deconvolution does not change the average semblance, attenuating those frequencies where the noise is most adverse will

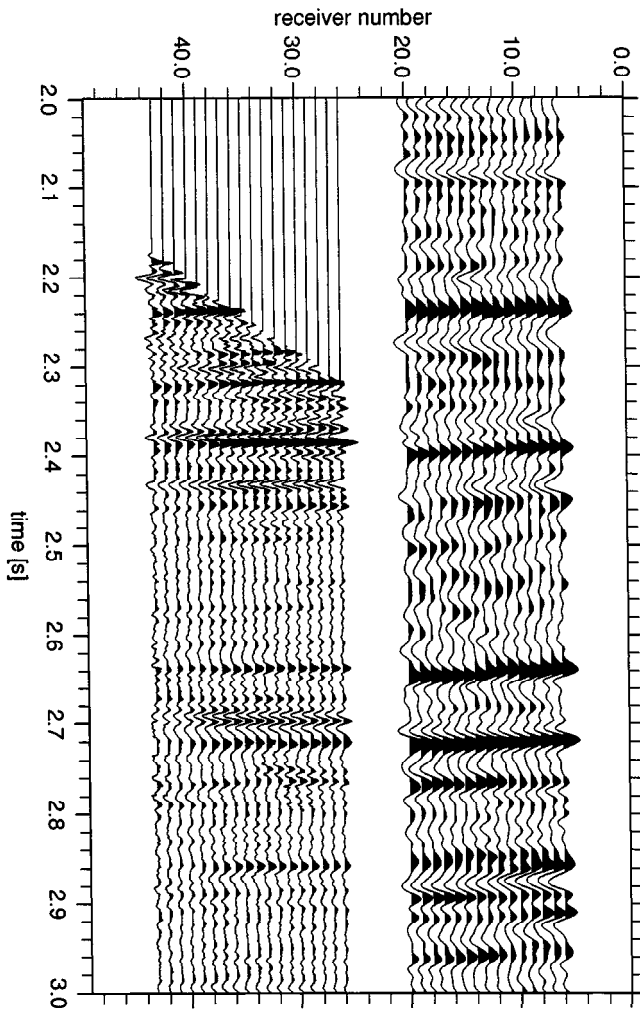


FIG. 15. "Look-ahead" image obtained from a VSP over depths ranging from 3500 to 3850 m. The data are displayed in two-way time with a portion of the surface seismic image immediately to the north of the well. The deepest receiver position corresponds to 2.4 s two-way time.

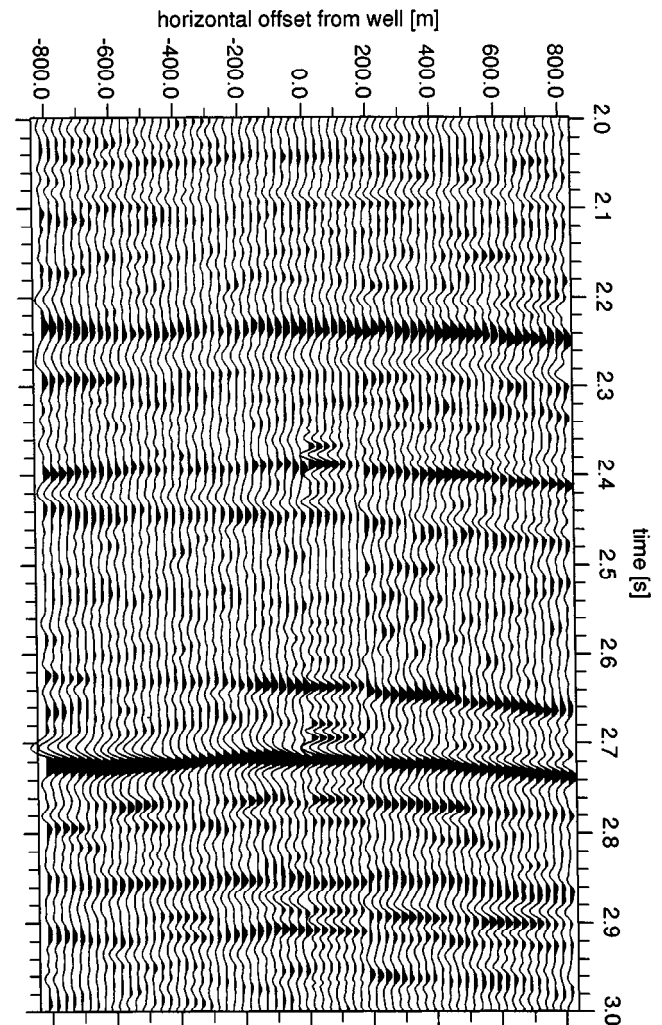


FIG. 16. Image obtained from processing a walkaway VSP data set. The acquisition was done in the cased hole using an array of eight magnetically clamped geophones. The shallowest level was at 3525 m, the deepest at 3630 m. The vibrator source was run along a north-south line from about 600 m to the south to about 2400 m to the north of the well. The VSP image covers the region between 0 and 175 m in offset and 2.35 and 3.0 s in two-way time.

improve the ratio between average signal energy and average total energy.

In Table 2 we have estimated the relative signal energy, before and after deconvolution, using the expressions from Table 1, as well as the average semblance using equation (13). The iterative repicking of the break times improves the average semblance by a factor of 4 from 0.015 to 0.066 and the relative signal energy by a factor of 1.3. In comparison, the deconvolution improves the relative signal energy by a factor of about 150. This dramatic change is related to the difference in the spectra of E_T and S seen in Figures 6 and 11.

The relative signal energy in the raw data is the average of the energy-weighted semblance (Table 1). That the energy-weighted semblance is small compared to the unweighted, average semblance S_0 (by a factor of 55) means that the semblance $S(\omega)$ is small when the total energy $E_T(\omega)$ is

large. In the deconvolved data, the relative signal energy is the semblance-weighted average semblance. This difference in accentuation as a result of deconvolution gives the significant improvement by a factor of 150 in the signal energy ratio for the drill-noise data. For the vibroseis walk-away VSP, the improvement from deconvolution was only about 2%. From these numbers, the deconvolved drill-noise data can also be seen to have more than twice the noise energy compared to the deconvolved vibroseis walk-away data.

Table 3 shows that the effective bandwidth, given by equation (18), of the drill-noise data is significantly less than what can be achieved using more conventional VSP sources. The disadvantage of less resolution must be weighed against the convenience of not having to disrupt the drilling operation. It may also be easier from local permitting considerations to accept geophones rather than surface seismic sources such as dynamite or vibroseis.

Comparison to reference deconvolution

We use the accelerometer for data compression and to calibrate the time. The data compression is based on the assumption that the transfer function between the radiating source signature and the accelerometer trace is constant during each period in which data is stacked (5 m of drilling). The timing calibration procedure assumes that the correlation function between the accelerometer-based and array-based signatures peaks at a time corresponding to the transmission time of extensional waves through the drill string.

In their work, Rector et al. (1988) and Rector and Marion (1991) use accelerometers mounted on the top of the drill string for their estimate of the seismic signature of the drill bit. We will compare the focused, optimal deconvolution processing described in this paper with the reference deconvolution technique described by them.

From equations (17) and (A-9), we see that the reference correlation effectively replaces the radiated signal $f(\omega)$ by $f'(\omega) = T^*(\omega)R(\omega)/|R(\omega)|^2 |f(\omega)|^2 e^{-i\omega t}$. The purpose of the deconvolution operator,

$$G'(\omega) = \frac{T(\omega)}{|T(\omega)|^2}, \quad (19)$$

suggested by Rector and Marion (1991) is to remove the drill-string transmission response T . The operator does not acknowledge or attempt to remove the drill-string reflection response R . The objective of the optimal deconvolution operator (7) is to reduce the radiated drill-bit signature to a unit impulse. The same may be achieved by the deconvolution operator (19) provided

- 1) The reflection response $R(\omega)$ of the drill string can be neglected.
- 2) $|f_b(\omega)|^2 = 1$ (For an experimental confirmation of this assumption, near-bit measurements of f_b is necessary. To our knowledge, such measurements have not been published. Any nonwhiteness in f_b will bias the estimate of T .)
- 3) $T(\omega)$ has no zeros. (Zeros may occur, depending on the actual location of the accelerometer, making T mixed phase. Neglecting this will bias the estimate of T .)

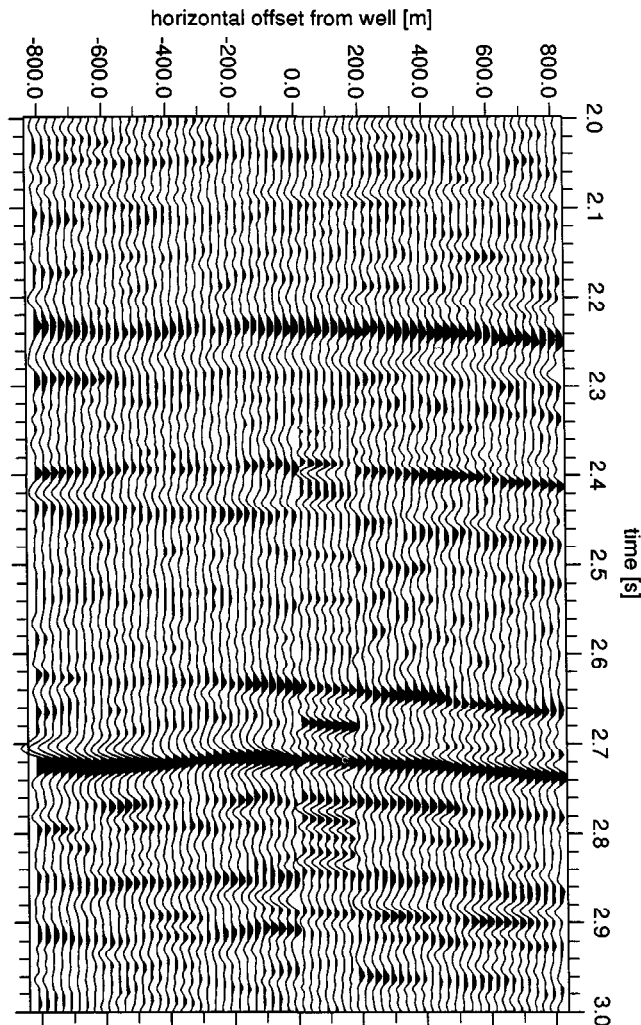


FIG. 17. The seismic image obtained from the optimally deconvolved drill-noise data. The north-south line was excluded because of the high level of residual noise close to the rig. The image from the five deconvolved east-west lines was projected on to the plane of the north-south going surface seismic line. The drill-noise image is shown superimposed on the image from the surface seismic data.

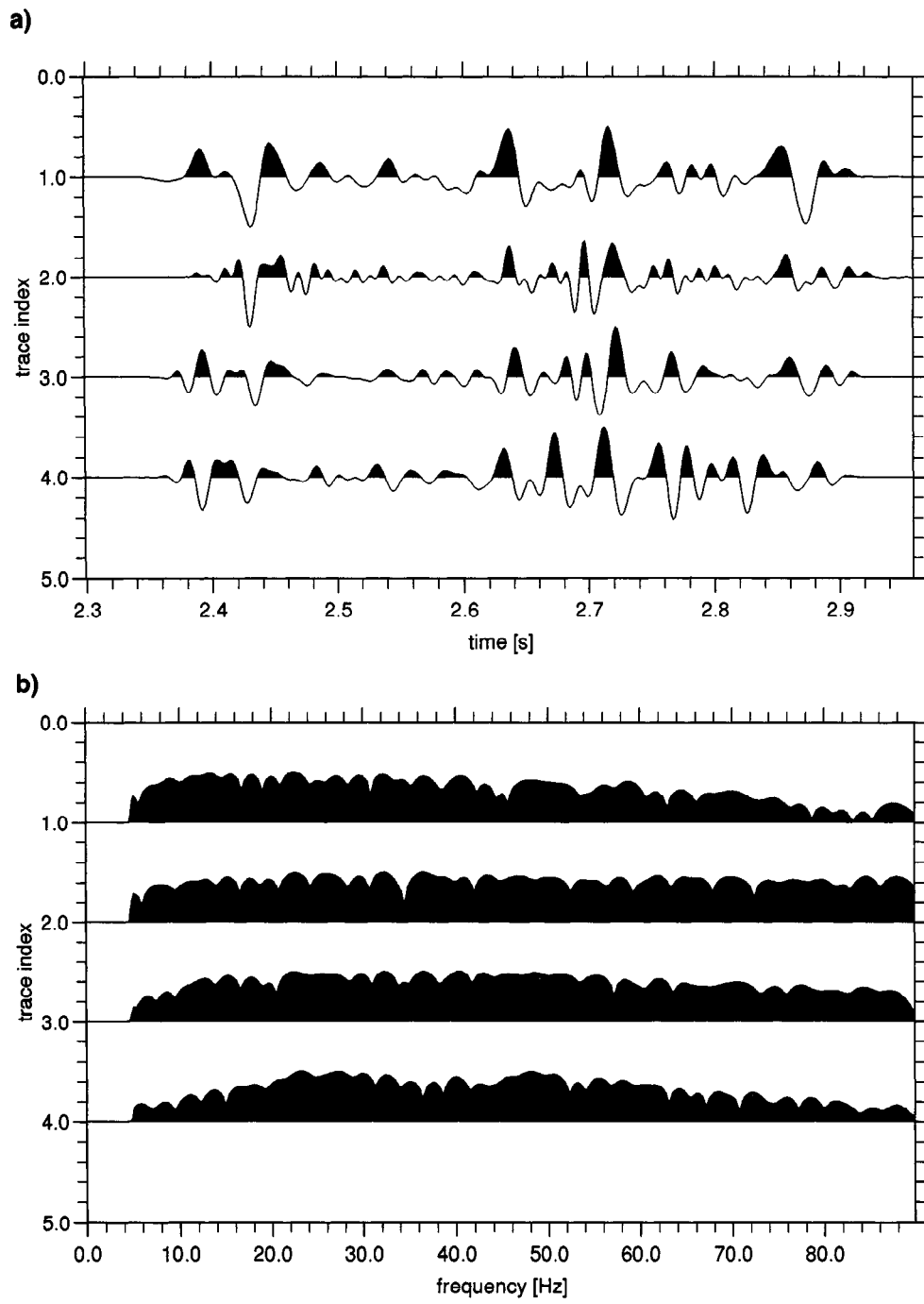


FIG. 18. Comparison of (a) traces and (b) spectra of "well traces," traces at the position of the borehole, from the four seismic images: trace 1: surface seismic, trace 2: zero-offset VSP, trace 3: walk-away VSP, and trace 4: drill-noise data.

If these conditions are not met, additional deconvolution processing may have to be applied to the reference-deconvolved data. In Figure 19, we show the effect of applying the accelerometer-based deconvolution filter (19) to the correlated data. The reference-deconvolution improves the signal definition significantly. However, as no proper notice has been taken of the geophone noise in the design of this filter, it is not surprising that it results in a more noisy section than the noise-minimizing algorithm. One could be tempted to believe that by using reference deconvolution followed by the optimal deconvolution algorithm one would get an overall improvement. However, from equation (A-4) it follows that the optimal deconvolution algorithm applied to the data in Figure 19 will produce the same results as shown in Figure 8.

It is clear from Figures 4 and 5 that coherent noise is strongly present in the correlated data. It is unclear to us how this noise (i.e., energy unrelated to the drill-bit generated signal but consistently picked up by both accelerometers and geophones) will affect the estimation of, and in turn be affected by the application of, the operator (19). The noise may bias the estimate of drill-string transmission response derived from prediction error filtering of the accelerometer trace. If the estimate is unbiased and we find an essentially correct drill-string transmission response, the application of the operator (19) will not attenuate the noise. In contrast, the deconvolution filter (7) is designed to minimize the noise in the geophone traces that is not coherent with the radiated bit signal.

Table 2. Measures of relative signal energy in five hours of correlated data. The numbers are given for the frequency range 0-90 Hz and found using the expressions in Table 1. The initial estimates are calculated using the time delays found by semblance analysis. The deconvolution algorithm converged after four iterations of repicking the break times. The corresponding numbers for the vibroseis walk-away VSP have been included for comparison.

Relative signal measures	Drill-noise VSP		Vibroseis Walkaway VSP
	Initial	Final iteration	
Average semblance	0.015	0.066	
Raw signal-to-total energy	0.0009	0.0012	0.611
Filtered signal-to-total energy	0.13	0.17	0.625

Table 3. The fraction of the total energy $\alpha_{S/T}$ attributed to the directly transmitted signal in the optimally deconvolved data, and the effective bandwidth Ω_{eff} , compared to the conventional zero-offset and walk-away VSP. The results for the zero-offset and walk-away VSP are from Haldorsen et al. (1994).

	Drill-noise VSP	Vibroseis Walkaway VSP	Dynamite Zero-offset VSP
$\alpha_{S/T}$	0.17	0.62	0.95
Ω_{eff}	36 Hz	83 Hz	95 Hz

CONCLUSIONS

We have seen that the array-based algorithm for extraction and deconvolution of the seismic signature of the drill bit works under very adverse signal-to-noise conditions to give seismic images that compare well with images obtained from surface seismic and wireline data.

Rig accelerometer measurements provide additional information that may be essential for timing calibration. Data reduction achieved by field correlation and stacking using the accelerometer as a reference signal means that we can do near-continuous sampling in depth without being overwhelmed by the volume of data.

The effective bandwidth of drill-noise data is significantly smaller than what can be achieved with more conventional VSP techniques but is still comparable to the bandwidth of surface seismic data. The reduced resolution must be weighed against the advantage that seismic images may be produced in real time using measurements that are not interfering with the drilling process, and the convenience of being able to produce an image ahead of the drill bit whenever it is needed. Even when timeliness is not an issue, it may be desirable to use a downhole seismic source and surface receivers for a "reverse" VSP, either for environmental reasons or for acquiring an economic 3-D VSP.

ACKNOWLEDGMENTS

We are indebted to H.-J. Zoch of RWE-DEA and Prof. Dr. R. Marschall for collaboration in planning the experiment, as well as to colleagues at Schlumberger-Doll Research, Schlumberger Cambridge Research and Geco-Prakla for their help and encouragement, and to Claude Roulet whose support made it possible for us to complete the project. We would like to thank RWE-DEA, BEB, Mobil, Preussag, and WIAG for releasing the data for publication.

REFERENCES

- Haldorsen, J., Farmer, P., and Desler, J., 1992a, Method for vertical seismic profiling: U.S. Patents 5 148 407.
- Haldorsen, J., Miller, D., and Walsh, J., 1994, Multichannel Wiener deconvolution of vertical seismic profiles: *Geophysics*, 59, 1500-1511.
- Haldorsen, J., Miller, D., Walsh, J., and Zoch, H.-J., 1992b, A multichannel approach to signature estimation and deconvolution for drill-bit imaging: 62nd Ann. Internat. Mtg., Soc. Expl. Geophys., Expanded Abstracts, 181-184.
- Miller, D., Haldorsen, J., and Kostov, C., 1990, Methods for deconvolution of unknown source signatures from unknown waveform data: U.S. Patents 4 922 362.
- Miller, D., Oristaglio, M., and Beylkin, G., 1987, A new slant on seismic imaging: Migration and integral geometry: *Geophysics*, 52, 943-964.
- Rector, J. W., 1990, Utilization of drill bit vibrations as a downhole seismic source: Ph.D. thesis, Stanford University.
- Rector, J. W., and Hardage, B. A., 1992, Radiation pattern and seismic waves generated by a working roller-cone drill bit: *Geophysics*, 57, 1319-1333.
- Rector, J. W., and Marion, B. P., 1991, The use of drill-noise energy as a downhole seismic source: *Geophysics*, 56, 628-634.
- Rector, J. W., Marion, B. P., and Widrow, B., 1988, Use of drill-bit energy as a downhole seismic source: 58th Ann. Internat. Mtg., Soc. Expl. Geophys., Expanded Abstracts, 161-164.
- Staron, P., Gros, P., and Arens, G., 1985, UK Patent Application GB2173596A.

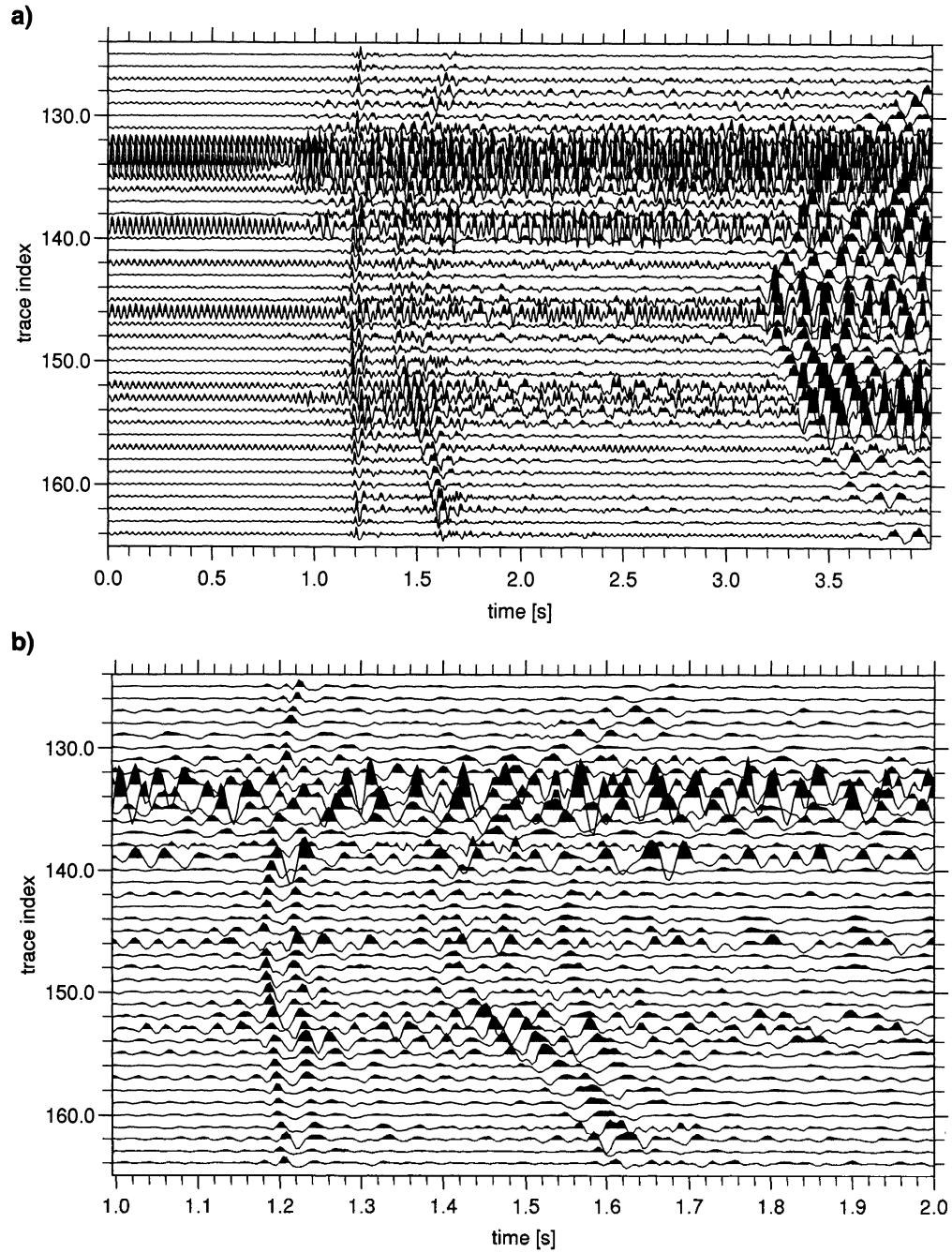


FIG. 19. The result of applying a deconvolution filter derived from the accelerometer according to equation (19). The 4 s and 1 s sections of data correspond to Figure 8.

APPENDIX A
DATA COMPRESSION BY REFERENCE CORRELATION

We will show that optimal deconvolution processing gives the same end result whether it is applied to correlated or uncorrelated data, provided the reference signal has no zeros in the frequency band of interest. We will argue that the correlated data may be stacked without significant loss of signal as long as the transfer function between the reference signal and the “true” bit signature is unchanged, and finally that as long as this transfer function has a time representation of limited duration, truncation of the correlated data may be done without significant loss of signal.

Finally, we will show how the timing calibration based on equation (17) has to be adjusted to be applied to data correlated with a reference signal.

Deconvolution

Correlation with a reference signal, s_a gives the following new set of traces:

$$s'_n(\omega) = s_a^*(\omega)s_n(\omega). \quad (\text{A-1})$$

Using equation (3), we find a new estimate of the source signal to be

$$f'(\omega) = s_a^*(\omega)f(\omega). \quad (\text{A-2})$$

From equations (8), (5), (9), (A-1), and (A-2), we see that $S'(o) = S(o)$, and the deconvolution operator to be applied to s'_n becomes [from equation (7)]

$$F'(\omega) = \frac{s_a(\omega)}{|s_a(\omega)|^2} F(\omega). \quad (\text{A-3})$$

Finally, from equations (A-1) and (A-3) we have

$$F'(\omega)s'_n(\omega) = F(\omega)s_n(\omega), \quad (\text{A-4})$$

-the same deconvolved traces independent of the reference correlation, provided that the reference signal has no spectral zeros. It follows, in particular, that we are insensitive to the difference between a reference accelerometer and a reference velocity sensor.

DATA COMPRESSION

As its derivation assumes that the complete waveforms have been kept after correlation, the relation (A-4) does not by itself provide any simplification or saving. A saving is only achieved if the correlated data may be truncated or stacked.

Setting

$$s_a(\omega) = T_{af}(\omega)f(\omega), \quad (\text{A-5})$$

where T_{af} is the transfer function between the “true” radiated seismic signature of the drill bit and the accelerometer, equation (A-1) can be rewritten as

$$s'_n(\omega) = T_{af}^*(\omega)f^*(\omega)s_n(\omega). \quad (\text{A-6})$$

The factor $f^*(\omega)s_n(\omega)$ represents an “optimal” reference correlation, replacing the source signature by its autocorrelation function. When both $T_{af}(\omega)$ and $f^*(\omega)s_n(\omega)$ are

unchanged, s'_n may be stacked without loss of essential information.

From equations (A-2) and (A-5) we find that the reference correlation effectively replaces the signature $f(o)$ by

$$f'(\omega) = T_{af}^*(\omega)|f(\omega)|^2. \quad (\text{A-7})$$

The correlated data can be truncated to the duration of f' plus a suitable listening time for reflected waves. In practice, truncation to 6 s does not appear to exclude any significant signal.

Using the model (14) for the accelerometer trace [adapted from Rector and Marion (1991)] and replacing the generated bit signal $f_b(\omega)$ by the radiated signal $f(\omega)$ by the substitution $f_b(\omega) = R^*(\omega)/|R(\omega)|^2 f(\omega)$ from equation (17), we get

$$T_{af}(\omega) \approx \frac{R^*(\omega)T(\omega)}{|R(\omega)|^2} e^{i\omega t_s} \quad (\text{A-8})$$

and

$$f'(\omega) = \frac{T^*(\omega)R(\omega)}{|R(\omega)|^2} |f(\omega)|^2 e^{-i\omega t_s}. \quad (\text{A-9})$$

Here, T and R are the transmission and reflection responses of the drill string. The complex exponential represents the propagation time delay through the drill string. T and R are both related to the geometry of the drill string and are expected to change when the drill string is changed. Therefore, the time it takes to drill 10 m of rock, corresponding to one drill-pipe segment, represents the maximum correlation and stacking interval.

The accelerometer mounted on the top of the drill string will, in addition to a colored and delayed version of the signal radiated from the bit, also record unrelated noise. The correlation of a geophone trace with a reference trace will concentrate energy present in both (signal and coherent noise). Noise that is randomly present on either (random noise) will remain spread out in time. The stacking of the geophone traces after correlation will attenuate random noise, whereas components like surface noise being recorded with a fixed time delay by both the reference accelerometer and the geophone will be consistently concentrated by the correlation and not be attenuated by the stacking. Provided it is spectrally separable from the array-based estimate of the radiated drill-bit signal, the optimal deconvolution of the stacked data is expected to attenuate the coherent noise.

The objective of the reference correlation, truncation, and stacking is to improve the signal-to-noise ratio without increasing the data volume. With a good reference signal the improvement in the energy ratio between signal and random noise is directly proportional to the data compression achieved by the operation (this assumes as a characteristic of the random noise that it is not compressed by the reference correlation). For drill-noise data, field correlation and stacking may mean a reduction in data volume by several orders of magnitude, concentrating hours of data acquisition to (in practice) a 6 s record.

Reference time

If we retain the full-waveform data for the accelerometer, we can find the vertical propagation time t_0 by inspecting the result of applying the filter $F(\omega) T(\omega) */ |T(\omega)|^2$ to the accelerometer trace. After correlation with the reference trace we have from equation (14), assuming $|f_b(\omega)|^2 = 1$ we have

$$s'_a(\omega) = |T(\omega)|^2. \tag{A-10}$$

Although it is impossible to reconstruct the drill-bit signature, we can still find the reference time t_0 . Assuming minimum phase, we find $T(\omega)$. By applying the filter F'

$T^*(\omega)/|T(\omega)|^2$ to the correlated accelerometer trace s'_a , and by using equations (A-3), (A-10), (5), (3), and (A-1) we get

$$F'(\omega) \frac{T^*(\omega)}{|T(\omega)|^2} s'_a(\omega) = \frac{f^*(\omega) f_b(\omega)}{E_T(\omega)} D_0(\omega) e^{i\omega(t_s - t_0)}. \tag{A-11}$$

With equation (17), this means that, independent of the reference correlation, the time reference t_0 can be found by shifting the peak of the accelerometer trace to the time t_s after the trace has been filtered by $T^*(\omega)/|T(\omega)|^2$ and deconvolved using the array-based deconvolution filter.

APPENDIX B

CONTRIBUTIONS FROM AUTOCORRELATION OF TRACES

The autocorrelation of the traces give an undesirable contribution to both the filtered data $F(\omega)s_n(\omega)$, and to the semblance $S(\omega)$. To see this, we rewrite $S(\omega)$. Inserting the expression (5) for $f_1(\omega)$ and (9) for $E_T(\omega)$ into equation (8), we get

$$S(\omega) = \frac{\left| \frac{1}{N} \sum_{n=1}^N s_n(\omega) e^{-i\omega \Delta t_n} \right|^2}{\frac{1}{N} \sum_{n=1}^N |s_n(\omega)|^2}$$

$$= \frac{\frac{1}{N^2} \sum_{n=1}^N |s_n(\omega)|^2}{\frac{1}{N} \sum_{n=1}^N |s_n(\omega)|^2}$$

$$+ \frac{\frac{1}{N^2} \sum_{n,k=1, n \neq k}^N s_n(\omega) s_k^*(\omega) e^{-i\omega(\Delta t_n - \Delta t_k)}}{\frac{1}{N} \sum_{n=1}^N |s_n(\omega)|^2}$$

$$= \frac{1}{N} + \frac{1}{N} \frac{\sum_{n,k=1, n \neq k}^N s_n(\omega) s_k^*(\omega) e^{-i\omega(\Delta t_n - \Delta t_k)}}{\sum_{n=1}^N |s_n(\omega)|^2}. \tag{B-1}$$

The first term, $1/N$, comes from the autocorrelation of s_n ; the second term from the crosscorrelation of different traces.

If the traces s_n contain only uncorrelated noise or the traces show very low correlation at time lags $(\Delta t_n - \Delta t_k)$, the difference in traveltimes for receivers n and k , the second term in equation (B-1) vanishes, giving

$$S_{auto}(\omega) = \frac{1}{N}. \tag{B-2}$$

This estimate of $S(\omega)$ approaches zero as $1/N$ as N goes to infinity. The autocorrelation term also contributes to the filtered data $F(\omega)s_n(\omega)$, giving a ghost signal along the moveout path t_n . In our implementation of the filter, the contribution from the autocorrelation term has been eliminated by excluding the trace n from $F(\omega)$ when applying it to $s_n(\omega)$.